Comput Visual Sci (2009) 12:397–408
DOI 10.1007/s00791-008-0125-x

Propagation and bifurcation of cracks based on implicit surfaces and discontinuous velocities

V. A. Kovtunenko · K. Kunisch · W. Ring

Received: 13 January 2005 / Accepted: 15 June 2007 / Published online: 15 July 2008

Abstract Cracks and their propagation with a given kinematic velocity are described as zero-level sets of a non-negative scalar function satisfying a transport equation. For smooth velocities this description is equivalent to a crack parameterization where the moving crack is obtained as the image of an initial reference crack under a coordinate transformation. Based on the implicit formulation, bifurcation type phenomena such as branching and merging of the crack, which cannot occur in the parameterized situation, are investigated numerically. Analytical and computational examples of the crack evolution with continuous as well as discontinuous velocities are presented in 2D and 3D domains.

Keywords Crack propagation · Bifurcation · Level set · Implicit surface · Velocity method

Mathematics Subject Classification (2000) 49J40 · 49Q10 · 49Q12 · 49L99 · 73M25

1 Introduction

The problem of the appropriate description of finite propagation or infinitesimal perturbation of geometric objects arises in various applications. Classical techniques are based on perturbations of the identity operator or (equivalently) on the velocity method. These techniques can be used for the description of homeomorphic displacements of geometric objects with regular boundaries and for the calculation of sensitivities of geometry dependent functionals [9,18,30].

Perturbation techniques in the context of crack perturbation are necessary, for example, in the framework of fracture mechanics for the determination of the direction and speed of propagation of cracks in solids [12,31,32]. It is generally accepted that a local fracture criterion involves the energy release rate at the crack tip, which can be expressed as the directional derivative of a potential energy functional [27]. Using shape sensitivity analysis for models in non-smooth domains with rectilinear cracks subject to inequality constraints, representations of the derivative were obtained in [16,17,19]. These considerations were based on perturbations of the identity operator and the corresponding coordinate transformations of domains with cracks.

In this paper, the description of cracks and their propagation motivates our interest in non-parameterized objects of Hausdorff dimension one in 2D and Hausdorff dimension two in 3D. This specifically includes non-closed, possibly branching curves in $\mathbb{R}^2$ or surfaces with non-empty boundaries in $\mathbb{R}^3$. In the case of cracks in three dimensions these boundaries correspond to crack fronts. We aim for describing the evolution of cracks including phenomena such as bifurcation of tips in $\mathbb{R}^2$ and bifurcation of crack fronts in $\mathbb{R}^3$. This motivates our choice of representing the crack by an implicit surface (the zero-level set of a *non-negative* time-dependent function ρ).

If the crack is defined by an implicit surface which is expressed as the zero level set of a non-negative function ρ propagated by a given vector field V, and all data are sufficiently smooth, then $\rho(t, y)$ satisfies

$$\rho_t + V\,\nabla\rho = 0. \qquad (T)$$

Communicated by G. Wittum.

V. A. Kovtunenko
Lavrent'ev Institute of Hydrodynamics,
630090 Novosibirsk, Russia

V. A. Kovtunenko (✉) · K. Kunisch · W. Ring
Institute for Mathematics and Scientific Computing,
University of Graz, Heinrichstr. 36, 8010 Graz, Austria
e-mail: victor.kovtunenko@uni-graz.at

We shall utilize the implicit formulation (T) also in the converse way. Given a family of cracks Γ_t, $t \geq 0$, it is quite natural to define $\rho^d(t, y) = \mathrm{dist}(y, \Gamma_t)$ as the corresponding level set function for which $\Gamma_t = \{y : \rho^d(t, y) = 0\}$. Solving the algebraic equation

$$\rho_t^d + V \nabla \rho^d = 0 \qquad (A)$$

for V, a natural extension of the velocity vector field (which a-priori is defined only on Γ) onto a neighborhood of the moving crack is obtained. Such an extension is a necessary ingredient for any kind of shape sensitivity analysis in the perturbation and in the level set context.

Traditionally level set methods are used for the evolution of dynamic surfaces with the velocity having non-zero component normal to the surface [5,14,21–23,28]. The situation is different here since crack propagation phenomena have zero normal component of the velocity, and only the tangential component is non-zero. This inherent specialty distinguishes the proposed method of an implicit surface description with the classical level set methods. The case of the tangential velocity is described by a transport Eq. T. For the normal velocity, the geometric variable is described as the zero level-set of a function ϕ (which is often chosen as the signed-distance function to the boundary of the shape variable) and propagated by solving an equation of Hamilton–Jacobi type:

$$\phi_t + V_n |\nabla \phi| = 0, \qquad (H\text{-}J)$$

where V_n is scalar velocity. It is easily seen that (H-J) is the specific case of (T) where $V = V_n n$ with a scalar velocity V_n and n the direction normal to the crack.

It is known that under appropriate conditions on V_n, the Hamilton–Jacobi equation (the "level-set equation") has a unique viscosity solution which exists for all times [8,20] in contrast to classical perturbation methods which are inherently local in time. The major advantage of the level set method lies in its flexibility, which allows to treat topology changes of the geometric variable in a unified way, and in its relatively simple implementation on fixed rectangular grids. Level set methods can also be used in a natural way to define shape perturbations and to obtain sensitivity results, as was observed in [6,13].

In this work, we are especially interested in geometric objects presenting *cracks*, i.e. subsets of $\mathbb{R}^N$ with Hausdorff dimension $N-1$. General $N-1$-dimensional sets are not easily described by classical level-sets where generically the zero level set of a smooth function is the boundary of an open set, i.e. an $N-1$-dimensional submanifold of $\mathbb{R}^N$ without boundary which divides $\mathbb{R}^N$ into an interior and an exterior region. The description of geometrical phenomena such as T-junctions or manifolds with boundaries usually requires the use of more than one level-set function. In this paper, we aim for a unified approach for the implicit (level-set like) description of general $N-1$ dimensional objects which propagate in time.

We recall the seminal work of Osher and collaborators [4] in which vector-valued level set functions were proposed as a technique to describe the evolution of surfaces with codimension higher than one. This is a very powerful approach for the description of the evolution of surfaces without boundaries with the goal of preserving merging and breaking properties. In [34] vector valued level set functions were proposed for the description of the evolution of cracks. This approach was combined with a maximum-hoop-stress criterion to determine the direction of the movement of the crack tip. However, it is not primarily geared towards bifurcation type phenomena.

Vector-valued level set functions were studied earlier in [2,3] with the goal of analyzing well-posedness. From the analytical point of view, the vector valued approach is difficult since it leads to a system of partial differential equations for which no maximum principle is available. This would be necessary for the viscosity sub- and super-solution concepts to apply. Therefore, the authors in [2,3] introduced a single non-negative level set function for the representation of the propagating surface. Here we utilize the same approach but focus on its numerical realization. We shall address potential difficulties related to the accurate determination of the location of the zero level set. Our numerical strategy involves a sharpening procedure for its correct determination without "thickening" phenomena as observed in [4].

In Sect. 2, the construction of extension velocities (A) for certain families of moving cracks are given, and the equivalence between the implicit formulation (T) and the propagation of the crack via coordinate transformation methods are proved. The corresponding transformation function and its inverse are constructed as the solutions of non-linear ODEs and transport equations, respectively, where the method of characteristics is used to establish the connection. In Sect. 3, numerical calculations of the propagation of cracks with given velocities are presented in 2D and 3D domains including bifurcating cracks. We compare two algorithms, where one is based on solution of ODEs and the other is based on the transport Eq. T. The algorithms are realized by high-accurate Runge–Kutta and WENO schemes, respectively, see [24,15].

2 Cracks and their propagation based on implicit surfaces

In this section, we discuss the use of scalar non-negative functions to describe the movement of cracks with a given velocity. We also relate the implicit surface description to the classical formulation of crack movement using coordinate transformations induced by velocity vector fields. The

implicit approach is more general since it allows discontinuous velocity vector fields describing topology changes such as branching and merging of crack branches.

Consider at time $t = 0$ the crack Υ_0 as a compact subset of $\mathbb{R}^N$, $N = 2$ or 3 with Hausdorff dimension $(N-1)$ and choose a continuous function $\rho_0 \geq 0$ such that

$$\Upsilon_0 = \{x \in \mathbb{R}^N : \rho_0(x) = 0\},$$
$$\mathbb{R}^N \setminus \overline{\Upsilon}_0 = \{x \in \mathbb{R}^N : \rho_0(x) > 0\}. \tag{1}$$

The distance function $\rho_0(x) = \inf_{y\in\Upsilon_0} |x-y|$, for instance, which is Lipschitz continuous in $\mathbb{R}^N$ (see [9,Theorem 2.1, p. 154]) serves this purpose. To describe the movement of the crack we choose a velocity field $V = V(t,x)$ and consider the transport equation (see [10]):

$$\begin{cases} \frac{\partial \rho}{\partial t}(t,y) + V(t,y)\,\nabla\rho(t,y) = 0, \\ \rho(0,y) = \rho_0(y). \end{cases} \tag{2}$$

Under appropriate conditions the solution to (2) satisfies $\rho(t) \geq 0$ and we can define the crack at time t by the implicit surface

$$\Upsilon_t = \{y \in \mathbb{R}^N : \rho(t,y) = 0\}. \tag{3}$$

It will be convenient to first recall the situation in the case of smooth vector fields. Below the subscript u denotes global uniform Lipschitz continuity of the elements in the respective function space.

Lemma 2.1 *Assume that $V = (V_1, \ldots, V_N) \in C([0,\infty); C_u^{0,1}(\mathbb{R}^N))^N$ and $\rho_0 \in C_u^{0,1}(\mathbb{R}^N)$ with $\rho_0 \geq 0$. For arbitrary $T > 0$ the Cauchy problem (2) has a unique solution $\rho \in C_u^{0,1}((0,T)\times\mathbb{R}^N)$ which satisfies (2) point-wise almost everywhere. Moreover, the solution has the form*

$$\rho(t,y) = \rho_0(R^{-1}(t,y)) \tag{4}$$

with an invertible mapping $R \in C^1([0,T]; C_u^{0,1}(\mathbb{R}^N))^N$ such that $R^{-1} \in C_u^{0,1}((0,T)\times\mathbb{R}^N)^N$. If $\rho_0 \geq 0$ we also have $\rho \geq 0$.

The proof is standard and can be based on the characteristic equations

$$\begin{cases} \frac{dR}{dt}(t) = V(t, R(t)), \\ R(0) = x. \end{cases} \tag{5}$$

We provide detailed arguments only for the regularity result stated in Lemma 2.1. Due to the regularity assumption on V and classical results on existence to dynamical systems, see, e.g. [9,Theorem 4.1], it follows that (5) admits a unique solution $R(t,\cdot)$ satisfying

$$R \in C^1([0,T]; C_u^{0,1}(\mathbb{R}^N))^N \quad \text{and} \quad R^{-1} \in C([0,T]; C_u^{0,1}(\mathbb{R}^N))^N. \tag{6}$$

It can be shown that

$$\rho(t,y) = \rho_0(R^{-1}(t,y)) \tag{7}$$

satisfies (2) almost everywhere on $(0,T)\times\mathbb{R}^N$. Moreover, setting $S(t,\cdot) = R^{-1}(t,\cdot)$, it follows that the components of S are solutions to the system of transport equations

$$\begin{cases} \frac{\partial S_i}{\partial t}(t,y) + V(t,y)\nabla S_i(t,y) = 0, & i = 1,\ldots,N, \\ S_i(0,y) = y_i, & i = 1,\ldots,N. \end{cases} \tag{8}$$

From this, we conclude that $R^{-1} \in C_u^{0,1}((0,T)\times\mathbb{R}^N)^N$. By differentiating the relation

$$y = R(t, R^{-1}(t,y)), \quad t \in (0,T) \tag{9}$$

with respect to y, an increase of smoothness in t is observed for the inverse function R^{-1} which must be compensated by a decrease of smoothness in y:

$$R^{-1} \in C^1([0,T]; L^\infty(\mathbb{R}^N))^N.$$

Thus, given a velocity field V, the solution to (2) describes the crack by means of (3) at time t and $y = R(t,x)$ provides the coordinate transformation between Υ_0 and Υ_t.

Conversely, given a time-dependent family of coordinate transformations $R(t,\cdot)$ which map a reference crack Υ_0 onto a family of moving cracks Υ_t and which satisfy (6) and $R(0,x) = x$, one can determine a velocity field and a function ρ such that the given family of cracks is described by the zero-level sets of ρ, where ρ and V satisfy (2). Indeed, such a velocity V is given by

$$V(t,y) = \frac{\partial R}{\partial t}(t, R^{-1}(t,y)). \tag{10}$$

The function R is then a solution to problem (5), and R^{-1} to (8). When $\rho_0 \geq 0$ describes the crack Υ_0 as in (1), the function $\rho(t) \geq 0$ obtained from (7) describes the crack Υ_t by (3).

Concerning the propagation of cracks, the restriction of $V(t)$ from $\mathbb{R}^N$ onto the crack Υ_t determines its local direction of propagation. At all points where the crack is locally diffeomorphic to an $N-1$-dimensional hypersurface (possibly with boundary as, e.g. at a crack tip or crack front) the velocity can be decomposed into normal and tangential components. The former implies changes of the crack shape, and the latter describes its prolongation. Typically the analysis of cracks in fracture mechanics is concerned with the propagation of cracks preserving its previous shape. Pure tangential velocities yield crack propagation in the tangential direction.

The Lipschitz regularity assumption of Lemma 2.1 for V does not allow to use discontinuous velocities in the classical situation where the implicit formulation and the use of coordinate transformations are equivalent. If we want, however, to describe phenomena such as the splitting or merging of cracks the use of velocities which are discontinuous, e.g. at

the splitting point becomes necessary. The implicit formulation (2) allows generalizations where discontinuous velocity field are admitted as long as they satisfy the Filippov condition

$$(x-y)\cdot(V(t,x)-V(t,y)) \geq -K(t)|x-y|^2, \quad \text{with} \quad K \in L^1(0,T). \tag{11}$$

This concept was introduced in [7,11] and it was shown that solutions to (2) and (5) in the sense of Filippov are well-defined and enjoy the backwards uniqueness property. The vector-field $V(x_1,x_2)=(1,\mathrm{sign}(x_2))$, for example, is not continuous but it satisfies (11). Condition (11) was generalized in [25], in the sense of ℓ^p-monotonicity yielding locally Lipschitz continuous solutions to the linear transport Eq. 2. These results imply that (7) is still well-defined for a much larger class of admissible velocities and that $\rho(t,y)\geq 0$ if $\rho_0 \geq 0$. For measure theoretic solution concepts, still based on the method of characteristics and preserving non-negativity in the sense that $\rho_0 \geq 0$ implies $\rho(t)\geq 0$ we refer to [26].

2.1 Analytic example

In the following analytic example we start with a given family of cracks $\Upsilon_t \subset \mathbb{R}^3$ and successively construct a corresponding implicit representation $\rho(t,\cdot)$ and a vector field V. Conversely, we show that this V reproduces the given propagation of Υ_t in the implicit formulation (2). In this example, we show that certain singularities (kinks in the crack front) can occur already in the comparably regular case of Lipschitz continuous velocity fields.

Let us consider as a specific example the family of non-planar cracks defined by

$$\Upsilon_t = \{y\in Q: \quad y_1 \leq \phi(t,y_3),\ y_2=\psi(y_1,y_3),\ 0\leq y_3\leq Y\},\quad t\geq 0,$$

with $\phi \in C^1([0,\infty);C_u^{0,1}(\mathbb{R}))$ and $\psi, \frac{\partial\psi}{\partial y_1}\in C_u^{0,1}(\mathbb{R}^2)$, and $Q=\mathbb{R}^2\times(0,Y)$. In Fig. 1 the geometrical situation is visualized for two different successive times t_1 and t_2.

The cracks can equivalently be expressed as

$$\Upsilon_t = \{y\in\mathbb{R}^3: \quad \rho(t,y)=0\}\cap Q$$

with

$$\rho(t,y)=[y_1-\phi(t,y_3)]^+ + |y_2-\psi(y_1,y_3)|.$$

To fulfill (2) the velocity field V has to satisfy

$$-\chi(y_1-\phi)\tfrac{\partial\phi}{\partial t} + \left(\chi(y_1-\phi)-\mathrm{sign}(y_2-\psi)\tfrac{\partial\psi}{\partial y_1}\right)V_1 + \mathrm{sign}(y_2-\psi)V_2 - \left(\chi(y_1-\phi)\tfrac{\partial\phi}{\partial y_3}+\mathrm{sign}(y_2-\psi)\tfrac{\partial\psi}{\partial y_3}\right)V_3 = 0$$

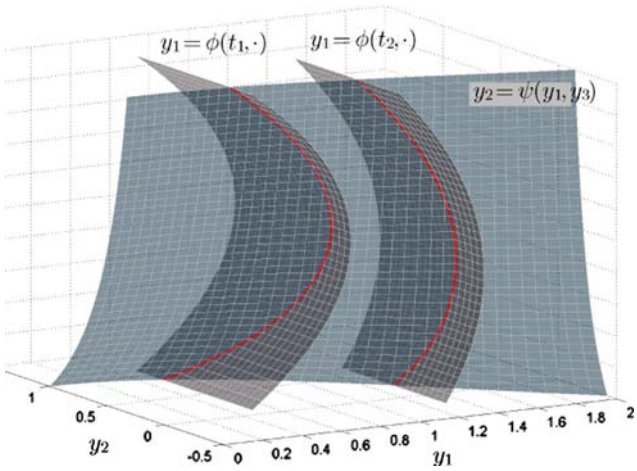

Fig. 1 Graph of ψ and graphs of ϕ for two different times t_1 and t_2

almost everywhere in $(0,T)\times\mathbb{R}^3$, where χ is the characteristic function of the set $\{x>0\}$. The velocity chosen as

$$V(y)=\left(\frac{\partial\phi}{\partial t},\frac{\partial\phi}{\partial t}\frac{\partial\psi}{\partial y_1},0\right)$$

satisfies the above relation and provides the corresponding coordinate transformation via (5) and (8) in the form

$$R(t,x)=\begin{pmatrix} x_1+\phi(t,x_3)-\phi(0,x_3)\\ x_2+\psi\,(x_1+\phi(t,x_3)\\ -\phi(0,x_3),x_3\,)-\psi(x_1,x_3)\\ x_3\end{pmatrix},$$

$$R^{-1}(t,y)=\begin{pmatrix} y_1-\phi(t,y_3)+\phi(0,y_3)\\ y_2-\psi(y_1,y_3)+\psi\,(y_1-\phi(t,y_3)\\ +\phi(0,y_3),y_3\,)\\ y_3\end{pmatrix}.$$

We note that also in the classical (non-Filippov) situation the regularity requirement of Lemma 2.1 admits singularities like finite corners at the crack front. Consider, for example, the velocity $V=(V_1,0,0)$ with $V_1(y)=[y_3-c]^+$, for some $c\in(0,Y)$. Then $V\in C_u^{0,1}(\mathbb{R}^3)^3$ and the cracks

$$\Upsilon_t=\{y\in Q: \quad y_1\leq\phi(0,y_3)+t[y_3-c]^+,\ y_2=0,\ 0\leq y_3\leq Y\}$$

exhibit a corner at $y_3=c$ on the crack front for every $t>0$.

3 Numerical calculations of the crack propagation

In this part we apply the theoretical results of Sect. 2 to calculate numerically the propagation of cracks with a given velocity. Based on the equivalent descriptions of moving cracks either by implicit surfaces (IS) or by coordinate transformations (CT) we suggest two corresponding algorithms

and compare them for several examples. The examples are constructed using tangential velocities to simulate tangential crack growth. A spiral-shaped crack, branching and merging cracks in $\mathbb{R}^2$, and a helicoid-shaped crack in $\mathbb{R}^3$ are presented.

The propagation of cracks in the continuous case was described in Sect. 2. Here we give a description of the corresponding finite-dimensional approximation and start with the choice of the discretization. Let Ω_h be a grid with mesh-size $h > 0$ in the bounded domain Ω, which for simplicity we assume to be time-independent. The continuous time-interval $[0, T]$ is discretized using a step-length $\Delta t > 0$ which is chosen in accordance with the CFL-condition for the transport Eq. T. The (unknown) crack Γ_t has co-dimension 1 in Ω and generally does not coincide with nodal points of Ω_h.

We formulate the following discrete problem of finding approximations Γ_t^s of the cracks Γ_t:

(P) *For the given discrete velocity*

$$V^h : \{k\,\Delta t \,:\, 0 \le k \le T/\Delta t\} \times \Omega_h \mapsto \mathbb{R}^N,$$

starting from the initial crack Γ_0^s at $t = 0$, located inside Ω, find the crack $\Gamma_{t_k}^s$ at all time-steps $t_k \in (0, T)$.

Here the initial crack Γ_0^s is represented either by a finite number of known points $x \in \mathbb{R}^N$ or as the zero level-set of an initial function ρ_0 for which the values on the grid Ω_h are supposed to be known.

3.1 The CT and IS based algorithms

Following the arguments on coordinate transformations in Sect. 2, we propose to solve (P) based on the first-order non-linear ODE system (5).

Algorithm CT

(0) *Set $k = 0$. Initialize the crack $\Gamma_{t_0}^s = \Gamma_0^s$ represented by the points $\{x_0^1, \ldots, x_0^l\}$.*
(1) *Set $t_k = k\,\Delta t$. If $t_k < T$ then go to step 2, else STOP.*
(2) *Find the velocity $V^h(t_k, x_k^j)$ for all $x_k^j \in \Gamma_{t_k}^s$, $j = 1, \ldots, l$ by interpolation from nearest grid points in Ω_h.*
(3) *Compute*

$$x_{k+1}^j = x_k^j + \int_{t_k}^{t_k+\Delta t} V^h(t_k, x(\tau))\, d\tau \quad \text{for all } x_k^j \in \Gamma_{t_k}^s \tag{12}$$

using a Runge–Kutta method.
(4) *Find the crack $\Gamma_{t_{k+1}}^s = \{x_{k+1}^j$ from (12)$\}$.*
(5) *Update $k = k + 1$, go to step 1.*

Velocities tangential to Γ_t preserve the previous crack shape. In this case, we update only the boundary points of the propagating crack in step (3) and we add the new boundary point to the set of existing crack points. This procedure is used in the numerical examples below.

In step 2 we use a linear interpolation of the velocity at $x \in \Gamma_{t_k}^s$ from nearest nodal points of the grid Ω_h. For the numerical integration of (12) we suggest a third-order Runge–Kutta method of the form:

$$\begin{aligned} &y^{(i)} = (1-\alpha_i)y^{(0)} + \alpha_i\left(y^{(i-1)} + \Delta t\, V^h(t_k, y^{(i-1)})\right)\\ &(i = 1, 2, 3), \quad x_{k+1}^j = y^{(3)}, \quad y^{(0)} = x_k^j,\\ &\alpha_1 = 1, \quad \alpha_2 = \frac{1}{4}, \quad \alpha_3 = \frac{2}{3}. \end{aligned} \tag{13}$$

This makes it necessary to interpolate the velocity also at the auxiliary points $y^{(i-1)}$ in (13).

Second, we utilize the implicit description of cracks (1), (3) to solve (P) and formulate the following algorithm based on the solution of the transport Eq. 2. Computationally it is difficult to determine accurately the zero-level of the fixed-sign function ρ in (3). Hence, below we introduce the concept of shadow of a crack, which consists of the nodal points within an ε-neighborhood of the crack.

Algorithm IS

(0) *Set $k = 0$, start with the non-negative distance function: $\rho^h(t_k, x) = \operatorname{dist}(x, \Gamma_0^s)$ for all $x \in \Omega_h$.*
(1) *Set $t_k = k\Delta t$. If $t_k < T$ then go to step 2, else STOP.*
(2) *Define the discrete gradient $\nabla^h \rho^h(t_k, x)$ for all $x \in \Omega_h$.*
(3) *Set $t_{k+1} = t_k + \Delta t$, compute $\rho^h(t_{k+1}, x)$:*

$$\rho^h(t_{k+1}, x) = \rho^h(t_k, x) - \int \frac{V^h(t_k, x)\nabla^h \rho^h(t_k, x)}{\Delta t} \quad \text{for all } x \in \Omega_h \tag{14}$$

using an appropriate numerical scheme.
(4′) *Resharpening: Restore the property that ρ^{sd} is the non-negative distance function of an $(n-1)$-dimensional crack by solution of an eikonal equation.*
(4) *Find the shadow of the crack:*

$$\Gamma_{t_{k+1}}^h(\varepsilon) = \{x \in \Omega_h : \quad \rho^{sd}(t_{k+1}, x) \le \varepsilon\}. \tag{15}$$

(5) *Update $t_k = t_{k+1}$, go to step 1.*

We now discuss some details of the algorithm. Numerical tests showed that the isotropic distance

$$\operatorname{dist}(x, \Gamma_0^s) = \min_{z \in \Gamma_0^s} \left(\sum_{j=1}^{N} (x_j - z_j)^2\right)^{1/2}$$

was preferable for the initialization in step 0 over an anisotropic choice of the norm in $\mathbb{R}^N$. The latter choice was convenient in the analytical constructions in Sect. 2 to obtain reference velocities.

For the discrete gradient ∇^h in step 2 we used a 5th-order accurate WENO-approximation based on 6-point finite difference left- and right-biased stencils, marked below with "−" and "+", respectively. In each coordinate direction x_j ($j = 1, \dots, N$) these approximations for the uniform grid are given by the following formula with respect to i-th nodal point [15]:

$$\frac{\partial^{\pm}}{\partial x_j}\rho_i = \frac{1}{12}(-\Delta^+\rho_{i-2} + 7\Delta^+\rho_{i-1} + 7\Delta^+\rho_i - \Delta^+\rho_{i+1}) \pm W(\Delta^-\Delta^+\rho_{i\pm2}, \Delta^-\Delta^+\rho_{i\pm1}, \Delta^-\Delta^+\rho_i, \Delta^-\Delta^+\rho_{i\mp1}) \tag{16}$$

with

$$\Delta^+\rho_m = \frac{1}{h}(\rho_{m+1} - \rho_m), \quad \Delta^-\Delta^+\rho_m = \frac{1}{h} \times(\rho_{m-1} - 2\rho_m + \rho_{m+1}),$$

$$W(c_1, c_2, c_3, c_4) = \frac{1}{3}\omega_0(c_1 - 2c_2 + c_3) + \frac{1}{12}(2\omega_2 - 1)(c_2 - 2c_3 + c_4),$$

$$\omega_0 = \alpha_0(\alpha_0 + \alpha_1 + \alpha_2)^{-1}, \quad \omega_2 = \alpha_2(\alpha_0 + \alpha_1 + \alpha_2)^{-1},$$

$$\alpha_0 = (\epsilon + i_0)^{-2}, \quad \alpha_1 = 6(\epsilon + i_1)^{-2}, \quad \alpha_2 = 3(\epsilon + i_2)^{-2},$$

$$i_0 = 13(c_1 - c_2)^2 + 3(c_1 - 3c_2)^2, \quad i_1 = 13(c_2 - c_3)^2 + 3 \times (c_2 + c_3)^2,$$

$$i_2 = 13(c_3 - c_4)^2 + 3(3c_3 - c_4)^2, \quad \epsilon = 10^{-6}.$$

Moreover, a finite-difference approximation of the gradient requires an extension $\widetilde{\Omega}^h$ of the grid Ω_h outside Ω. For the suggested 7-point central scheme a linear extension of ρ onto 3 points in each direction outside Ω_h was used.

We realized the finite-difference approximation of (14) by a Lax–Friedrichs flux. Various fluxes of upwind and Godunov type were tested. They show comparable performance when the derivative with respect to space variables is approximated by the WENO-scheme. For the Lax–Friedrichs flux (14) takes the form:

$$\rho^h(t_{k+1}, x) = \rho^h(t_k, x) - \int \sum_{j=1}^{N} \left\{ V_j^h(t_k, x)\frac{1}{2}\left(\frac{\partial^+}{\partial x_j} + \frac{\partial^-}{\partial x_j}\right) \times \rho^h(t_k, x) - \max_{x\in\Omega_h} \times \left(V_j^h(t_k, x)\right)\frac{1}{2}\left(\frac{\partial^+}{\partial x_j} - \frac{\partial^-}{\partial x_j}\right)\rho^h(t_k, x) \right\} \Delta t \tag{17}$$

with the "+" and "−" derivatives from (16).

The 3rd-order Runge–Kutta method was used for time integration in (17), too. Following the notation in (13) results in the following scheme for (14):

$$\rho^{(i)} = (1 - \alpha_i)\rho^{(0)} + \alpha_i \left(\rho^{(i-1)} - \Delta t \times \sum_{j=1}^{N} \left\{ V_j^h(t_k)\frac{1}{2}\left(\frac{\partial^+}{\partial x_j} + \frac{\partial^-}{\partial x_j}\right) - \max_{x\in\Omega_h}\left(V_j^h(t_k)\right)\frac{1}{2}\left(\frac{\partial^+}{\partial x_j} - \frac{\partial^-}{\partial x_j}\right) \right\} \rho^{(i-1)}\right) \times (i = 1, 2, 3), \quad \rho^h(t_{k+1}) = \rho^{(3)}, \quad \rho^{(0)} = \rho^h(t_k). \tag{18}$$

Again, step 2 is repeated by Runge–Kutta iterations (18) to define the discrete gradients $\nabla^h\rho^{(i-1)}$ according to (16).

Step 4′ is introduced to cope with the problem that the function ρ looses the property of being the distance function of a crack during the iteration of t_k. This includes the effect that the function $\rho(t_k)$ can become positive at points which should lie on the crack. Thus, detection of the zero level-set becomes an increasingly ill conditioned task as the crack evolves. To overcome this difficulty we suggest the following heuristic procedure:

- Shift the function ρ to obtain $\rho^d = \rho - d$ with a constant $d > 0$. The new function ρ^d has a zero-level set which includes the crack in its interior.
- Calculate the signed distance function ρ^{sd} to the zero level-set $\Gamma^d = \{\rho^d = 0\}$ by solving the eikonal equation

$$|\nabla\rho^{sd}| = 1 \tag{19}$$

with the boundary condition $\rho^{sd} = 0$ on Γ^d. Use a fast marching algorithm for the numerical solution [29,33].
- Shift $\rho^{sd} = \rho^{sd} + d$ to obtained the resharpened function ρ^{sd} as the non-negative distance function.

The heuristic idea behind the procedure described above is that the signed distance function of a "slim" set—the set Γ^d which includes the crack—contains a set of singularities inside, which is a good approximation of the actual crack. Moreover, if the thickness of the set is approximately constant, the value of the signed distance function along the set of singular points is also approximately constant. Although this set is not resolved explicitly, the crack is much better localized implicitly in the resharpened function than in the original representation.

In step 4 we do not define the crack $\Gamma_{t_{k+1}}$ but only its shadow $\Gamma^h_{t_{k+1}}(\varepsilon)$ as a subset of the grid points Ω_h. To determine the crack from its shadow an additional algorithmic step must be introduced. In our numerical tests a local piecewise-linear interpolation by a least-squares method was successful. Nevertheless, the interpolation procedure required to be

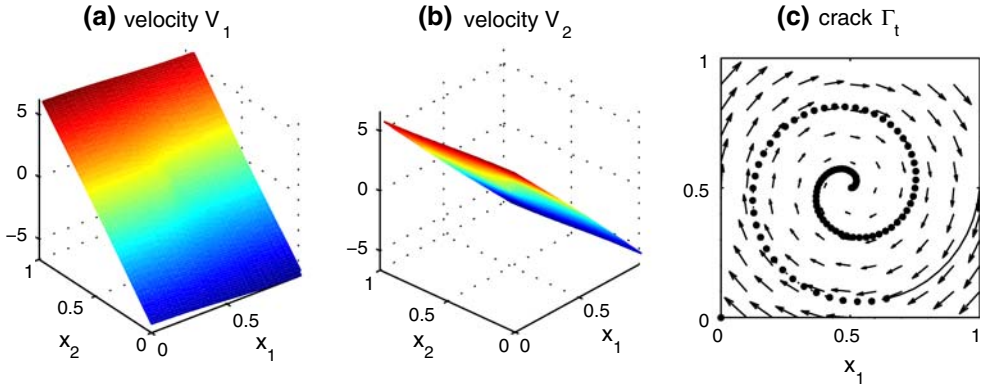

Fig. 2 The spiral-shaped crack obtained by Algorithm CT

handled interactively to obtain an appropriate performance of the crack in each particular example, and, therefore, it was not included in the algorithm.

Note that Algorithm IS is much more involved than Algorithm CT. If Algorithm CT is applicable it is simpler and more effective than Algorithm IS. However, Algorithm IS does not require a parameterization of the crack and hence has a broader scope. In the following examples we discuss situations where the use of each of the algorithms has certain advantages.

3.2 Numerical examples

To construct an example for (P) we choose a reference crack Γ_t and derive an analytical formula for the corresponding velocity V following the lines of Sect. 2. Then this velocity and an initial crack Γ_0 are taken for the initialization of both algorithms from Sect. 3.1. The computed cracks are then compared to the reference crack Γ_t.

Example 1 Spiral-shaped crack. Let us start with a smooth example of a spiral-shaped crack represented by a parametric curve in $\mathbb{R}^2$. In polar coordinates $(r, \phi) \in [0, \infty) \times \mathbb{R}$ we define the crack Υ_t for $t \in [0, 1 - t_0)$ with fixed $0 < t_0 < 1$ as

$$\Upsilon_t = \{r = A(1-s), \phi = \kappa(1-s) \text{ for } s \in (-\infty, t_0 + t)\}, \tag{20}$$

for given positive constants A, κ. Let Ω be the unit square $\{(x_1, x_2) \in (0, 1)^2\}$. For a cartesian representation of the crack points we set

$$x_1 = 0.5 + r\cos\phi, \quad x_2 = 0.5 + r\sin\phi.$$

Following (20), Γ_t is given as

$$\Gamma_t = \left\{ \begin{pmatrix} x_1 \\ x_2 \end{pmatrix} = \begin{pmatrix} 0.5 + A\,(1-s)\,\cos\left(\kappa(1-s)\right) \\ 0.5 + A\,(1-s)\,\sin\left(\kappa(1-s)\right) \end{pmatrix} \right. \\ \left. \text{for} \quad s \in (-M, t_0 + t) \right\}, \quad t \in (0, 1 - t_0), \tag{21}$$

where $M > 0$ is a sufficiently large number to exclude interference of the "tail" of the crack with the behavior at the moving crack tip in the numerical realization. We set the concrete parameters as $A = 0.5$, $\kappa = 4\pi$, $t_0 = 0.1$. In Cartesian coordinates, the velocity has the form

$$\begin{pmatrix} V_1 \\ V_2 \end{pmatrix} = \begin{pmatrix} -Ar^{-1}(x_1 - 0.5) + \kappa(x_2 - 0.5) \\ -Ar^{-1}(x_2 - 0.5) - \kappa(x_1 - 0.5) \end{pmatrix}, \tag{22}$$

where $r = ((x_1 - 0.5)^2 + (x_2 - 0.5)^2)^{1/2}$.

We choose a uniform grid Ω_h for the discretization of Ω and we define the discrete vector field V^h as the restriction of V given in (22) to the grid points in Ω_h. The two components of this time-independent velocity are illustrated in Fig. 2a, b, respectively. In Fig. 2c the velocity field is displayed as a vector field in the plane and the initial Γ_0 is depicted as a solid-line.

With these data we first solve (P) using Algorithm CT. Choosing $h = 0.01$ and $\Delta t = 0.01$ we calculate the propagation with velocity V^h of the crack-tip, starting with the tip of Γ_0 as initial value. The time interval is chosen as $(0, 0.9)$. For 90 time-steps, the points x_k obtained as solution to (12) are drawn as a sequence of dots in Fig. 2c. For comparison the reference crack Γ_t (as defined in (21)) for $t = 0.9$ is drawn as a dashed line. It is seen that the dots coincide very well with the dashed line.

We next test Algorithm IS with $h = 0.01$ and $\Delta t = 0.001$ for this example. The numerical results are presented in Fig. 3a, b for the initialization, and in Fig. 3c, d after 900 time-iterations. The following quantities are depicted: the Euclidian distance function ρ_0 to Γ_0^s, the shadow $\Gamma_0^h(\varepsilon)$ of the initial crack with $\varepsilon = h$, the solution ρ to (18) at $t = 0.9$, and the corresponding shadow of the crack with $\varepsilon = h$. The reference cracks are plotted as solid lines in Fig. 3b, d. As in the case of the (CT)-algorithm, the quality of approximation of the actual movement of the crack is quite satisfactory. The solid line (the actual crack) is well contained within the computed shadow.

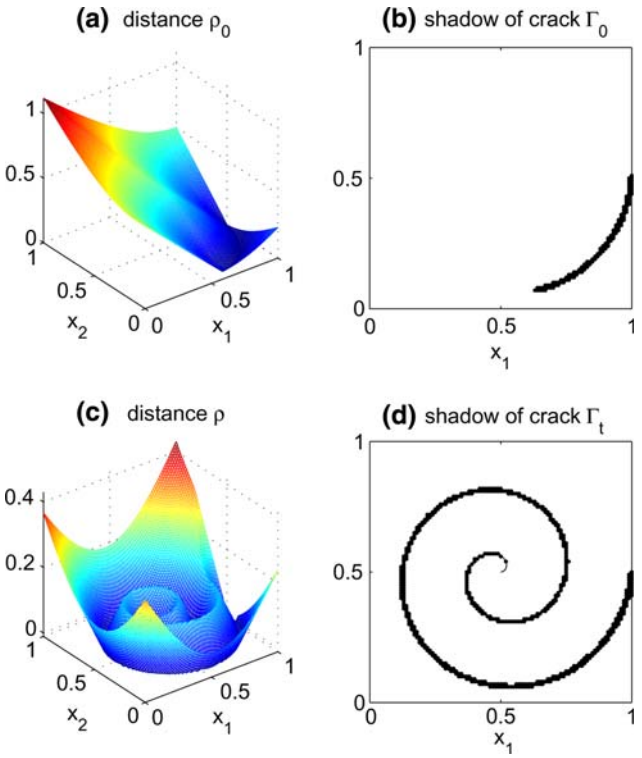

Fig. 3 The spiral-shaped crack obtained by Algorithm IS

In all the examples we used the resharpening strategy with a down-shift parameter d which corresponds approximately to two times the mesh-size of the underlying grid. If d is chosen smaller then the fast marching algorithm used in the resharpening procedure may produce unstable results. We note that for this example, the improvement by including the resharpening procedure in the overall algorithm is considerable. Without resharpening the thickness of the shadow region increases during the propagation.

At this point, a comment on the role of the velocity V is indicated. For the implicit formulation (IS), more specifically for the solution of the transport Eq. 14 it is necessary to have a globally defined velocity function. In contrast, the velocity for the propagation of a parameterized crack (12) needs to be defined only at the crack tip (more precisely in some neighborhood of the crack tip, since the Runge–Kutta scheme requires knowledge of the velocity vector field on intermediate auxiliary points). In practice the local direction for propagation of the crack tip is found by using a model for the local energy release generated by the growing crack. In this situation a global velocity is, however, not immediately at hand. In the following, we present an algorithmic extension of a known velocity (multi-valued in the case of crack-splitting) given only at the crack tip to a globally defined velocity which leaves the previously obtained crack shape invariant. An analogous situation frequently occurs when an interface is propagated using level-set techniques. There, the speed of propagation is often defined only on the interface and needs to be extended onto a neighborhood of the interface to enable the level-set methodology to work. See [1] and [22,Chap. 8] for details of the construction of extension velocities.

We also want to adopt the "level-set philosophy" of working only with data on a fixed regular grid and to avoid interpolation to sub-grid level as much as possible in our implicit approach (IS). We therefore assume that the velocity of the crack tip is given on one (or possibly several) grid point(s) close to the crack tip and we start the extension procedure with these data.

Suppose now that the velocity vector $V_{t_k}^{\mathrm{tip}}$ is given only at a regular grid point close to the tip $\Gamma_{t_k}^{\mathrm{tip}}$ of a propagating crack Γ_t at time $t = t_k$. Suppose moreover that an approximation $\widetilde{\Gamma}_{t_k}^{\mathrm{tip}}$ of the position of the crack tip is known. The velocity extension is inserted before step 3 in Algorithm IS:

- Define

$$\Omega_u(t_k) = \left\{ x \in \Omega : \quad \mathrm{dist}(x, \widetilde{\Gamma}_{t_k}^{\mathrm{tip}}) = \mathrm{dist}(x, \widetilde{\Gamma}_{t_k}) \right\};$$

- Extend

$$V(t_k, x) = \begin{cases} V_{t_k}^{\mathrm{tip}} & \text{if } x \in \Omega_u(t_k), \\ V(t_{k-1}, x) & \text{otherwise.} \end{cases} \tag{23}$$

The construction of the extension is based on a splitting of the reference domain Ω into two subdomains. We refer to the first domain $\Omega_u(t_k)$ as the update domain where actual movement of the crack tip takes place. The update domain is the set of points for which the closest point on the crack is the crack tip. It can easily be checked whether or not a grid point belongs to the update region by comparing the actual distance to $\tilde{\Gamma}_{t_k}^{\mathrm{tip}}$ with the value of the distance function ρ^{dist} to the crack Γ_{t_k}. The distance function is obtained as a by-product of the resharpening procedure in step $4'$ and can be computed in logarithmic time using a fast marching algorithm. In the update domain the velocity field is set to the constant vector $V_{t_k}^{\mathrm{tip}}$. In the complementary domain the velocity is set to the velocity field obtained in the previous time-step. With this choice, the prior shape of the crack is preserved. This is due to the fact that the prior shape itself was obtained using the same (tangential) velocity vector field in the complementary domain. As initialization for the first time-step, we use $V(t_{-1}, x) = 0$.

Using this construction, points which are close to the crack tip and "in front of the tip" propagate with the same velocity as the tip itself. Remote points or points lying "behind the tip" are not effected by the update velocity and propagate according to the previously specified velocity. In Fig. 4, the splitting into two subdomains, the extended velocity and the propagating crack are shown at eight different time-instances. It

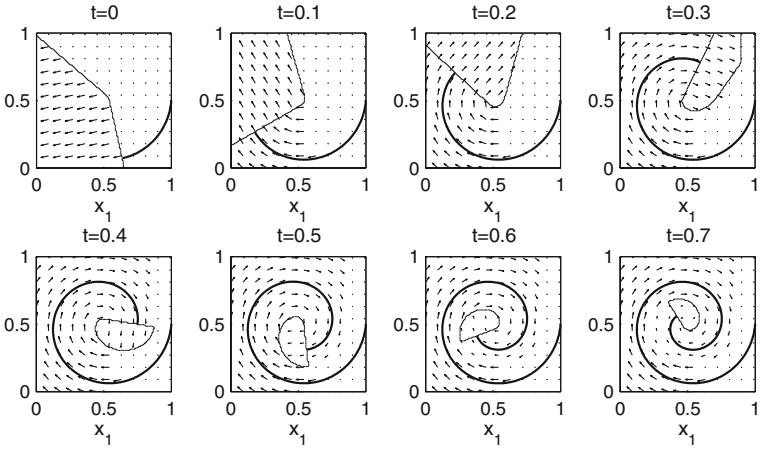

Fig. 4 Velocity field $V(t)$ extended from the velocity of the crack tip of spiral-shaped crack

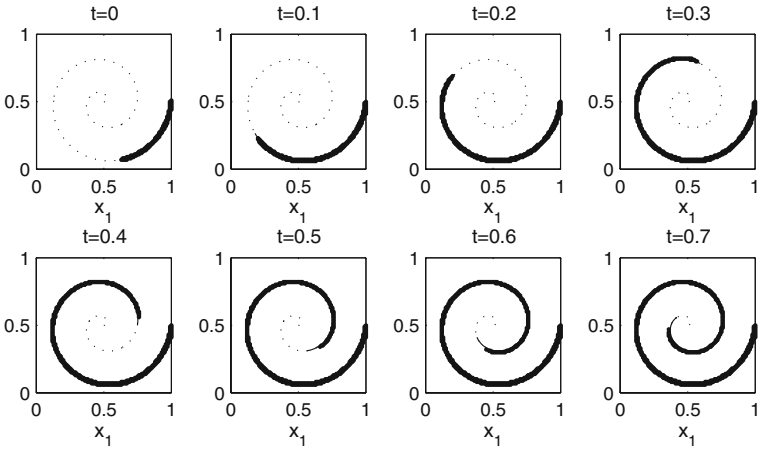

Fig. 5 The spiral-shaped crack obtained by Algorithm IS with the velocity extension procedure

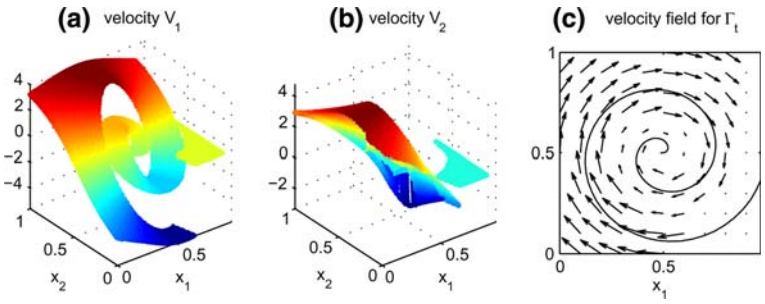

Fig. 6 The limit velocity V extended from the velocity of the crack tip of spiral-shaped crack

can be observed that the update domain is always in front of the crack tip.

For the numerical calculations shown in Fig. 4 we choose $\widetilde{\Gamma}^{\mathrm{tip}}_{t_k}$ close to the reference crack tip $\Gamma^{\mathrm{tip}}_{t_{k+1}}$. The latter is found by solving the discrete ODE system (12) at $\Gamma^{\mathrm{tip}}_{t_k}$. Nevertheless, $\widetilde{\Gamma}^{\mathrm{tip}}_{t_k}$ and $V^{\mathrm{tip}}_{t_k}$ can be determined on the fixed grid points of Ω^h without precise tracking of the reference crack. In the example of the spiral-shaped crack we obtain $V^{\mathrm{tip}}(t)$ from the analytical representation (22). The numerically extended velocity field $V(t,x)$ and the sets $\Omega_u(t)$ where $\mathrm{dist}(x,\widetilde{\Gamma}^{\mathrm{tip}}_t) = \mathrm{dist}(x,\widetilde{\Gamma}_t)$ are plotted in Fig. 4 at points $t = 0, 0.1, \ldots, 0.7$. Realization of Algorithm IS with the velocity extension procedure gives the distance function $\rho(t)$ and the respective shadows of crack Γ_t. The latter ones are depicted in Fig. 5 for the selected time points t. The limit of the piecewise-constant iterations of $V(t_k,x)$ in (23) for $k = 0,1,\ldots,[0.9/\Delta t]$ is depicted in Fig. 6. This time-independent velocity can be used for Algorithm IS, which in this case produces the same result as plotted in Fig. 5.

From the extension we get information how to construct a piecewise-constant velocity field when the tip of a crack is endowed with a multi-valued vector V^{tip} at some bifurcation point. The domain of propagation should be split into sectors

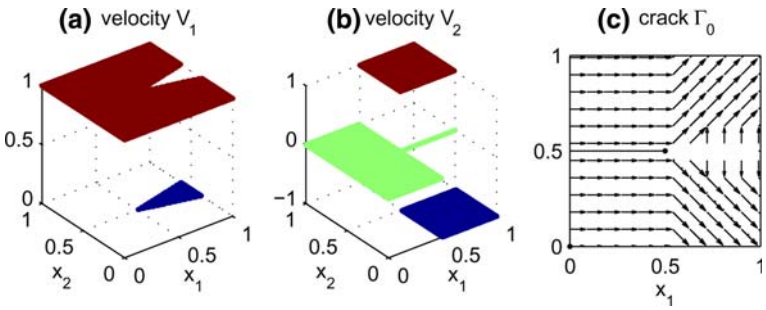

Fig. 7 Data for the branching crack

near the bifurcation point such that each value of $V^{\rm tip}$ can be extended into these sectors with the above procedure. This idea is realized in the next example.

Example 2 Branching crack. The second example deals with a non-smooth case of the branching (bifurcating) crack shown in Fig. 7c. The components V_1 and V_2 of the corresponding time-independent velocity are constructed as presented in Fig. 7a, b, respectively. The angle of the sector drawn in Fig. 7a is chosen as $2\arctan 1/4$. It can be taken arbitrarily within $(0, \pi/2)$. Note that such a discontinuous velocity is inadmissible in the context of the classical (non-Filippov) consideration. In the discrete space we start with the initial rectilinear crack $\Gamma_0 = \{0 < x_1 < 0.5, x_2 = 0.5\}$ depicted in Fig. 7c by a solid-line, which should follow during the time-iteration two rectilinear branches forming $\pm\pi/4$-angles with the line $x_2 = 0.5$ marked with dashed-lines.

Algorithm CT applied to this non-smooth example can follow only one of the branches. Alternatively, Algorithm IS gives good result as we can see in Fig. 8, where the solution ρ and the corresponding shadow of Γ_t are computed for $h = 0.01$ and $\Delta t = 0.001$ after 400 time-steps ($t = 0.4$). The solid-line in Fig. 8d represents the reference crack, whose branches are both closely surrounded by the computed crack shadow with $\varepsilon = h$.

The initialization of $\rho^h(t_0)$ should be taken precise enough such that the zero-level sets of $\rho^h(t_0)$ and ρ_0 from (2) are close to each other. Otherwise, the difference of $\rho^h(t_k)$ from zero increases with each iteration and results in a thickening of the shadow of the crack. For coarse or noisy initializations the construction principle presented in Algorithm IS should include an additional substep in Step 4′:

- Replace ρ by the updated (sharpened) function $\rho = \rho^{sd}$.

This substep restores the property that ρ is the non-negative distance function of the crack. Its use is successful for slow velocities and short time intervals. Otherwise it has the disadvantage that the boundary condition for the solution of the eikonal Eq. 19 cannot be implemented with high accuracy due to the very slim zero level-set of the shifted function ρ^d. This has the effect that the resharpening procedure partly neutralizes the propagation step of the WENO scheme. This may lead to a slower propagation than predicted analytically. This difficulty cannot be eliminated by a larger choice of d. In fact, increasing d gives a faster propagation but a shadow region which is not localized as well as in the case of small d. The quality of the shadow region is comparable to the result in which we skip the resharpening step 4′ completely and put $\rho^{sd} = \rho^h$ in (15).

Note that the function ρ^{sd} obtained with the resharpening process always has the form of a distance function and is, therefore, different from the function ρ obtained by time-stepping without resharpening. The zero level-sets, however, agree for both.

Example 3 Merging crack. For another non-smooth example we present a merging crack whose corresponding discontinuous velocity is depicted in Fig. 9. The velocity is cut off by

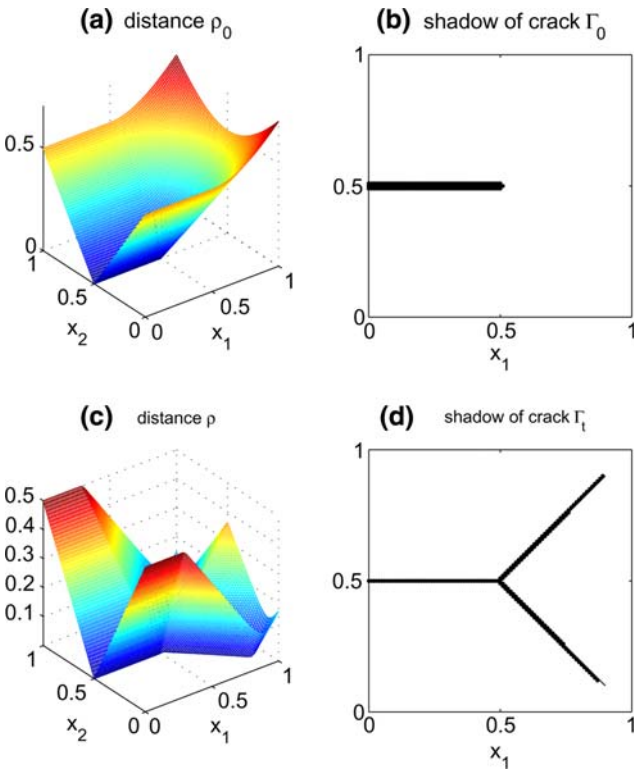

Fig. 8 The branching crack obtained by Algorithm IS

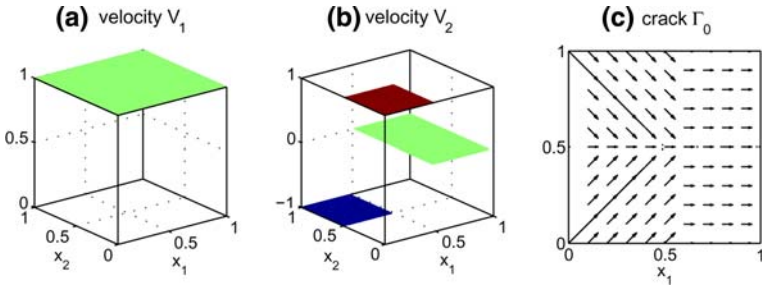

Fig. 9 Data for the merging crack

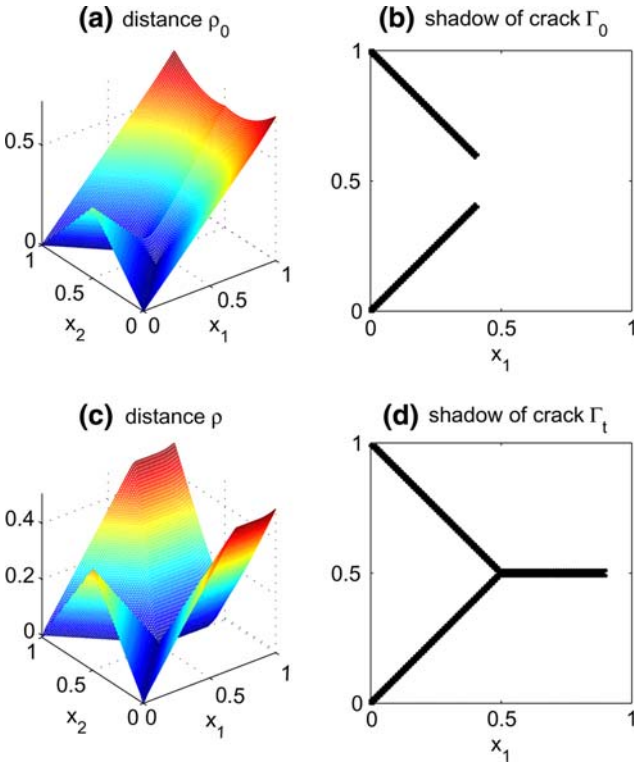

Fig. 10 The merging crack obtained by Algorithm IS

zero near the boundary $x_1 = 0$. In Fig. 10 we show: (a) the initial distance ρ_0, (b) the shadow of the initial crack Γ_0 with $\varepsilon = h$, (c) the distance ρ, (d) the shadow of Γ_t with $\varepsilon = h$, which is computed by Algorithm IS after 500 time-steps for $h = 0.01$ and $\Delta t = 0.001$. Since the shadow is very slim, the resharpening is not needed.

Example 4 Helicoid-shaped crack. Finally, we present a 3D-calculation. A helicoid-shaped crack within the unite cube $\Omega = \{(x_1, x_2, x_3) \in (0, 1)^3\}$ is considered. We define parametrically the unbounded surface Υ_t for $t \in [0, 1 - t_0)$ with fixed $0 < t_0 < 1$:

$$\Upsilon_t = \left\{ x \in \mathbb{R}^3 : \begin{cases} x_1 = s_1, \\ (x_2 - 0.5)\cos 2\pi s_1, \\ -(x_3 - 0.5)\sin 2\pi s_1 = 0, \end{cases} \right. \\ \left. \text{for } s_1 \in (-\infty, t_0 + t) \right\}.$$

The crack is illustrated in Fig. 11 for $t = 1$. Using arguments already presented above we construct the corresponding time-independent velocity

$$V = (1, 2\pi(x_3 - 0.5), -2\pi(x_2 - 0.5))$$

and cut it off by zero near $x_1 = 0$ to preserve the initial crack. The bounded crack Γ_t is defined in a cylinder inside Ω as follows:

$$\Gamma_t = \Upsilon_t \cap \{x_1 > 0\} \cap \{(x_2 - 0.5)^2 + (x_3 - 0.5)^2 < 0.5^2\}.$$

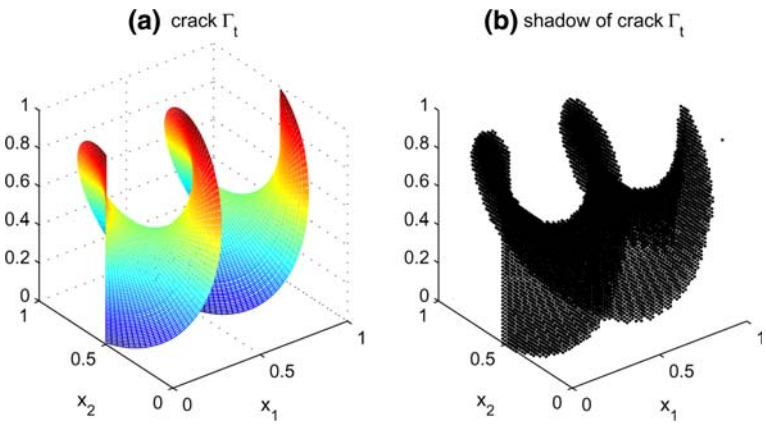

Fig. 11 The helicoid-shaped crack obtained by Algorithms CT and IS

For $T = 0.9$ we initialize with $t_0 = 0.1$ and parameterize the initial crack Γ_0 by two parameters: s_1 along the x_1-axis and s_2 in the planes $x_1 = s_1$, with uniform spacing Δs. In Ω we construct a uniform grid of mesh-size h and discretize the time-interval $[0, T]$ by uniform step-length Δt. For $h = \Delta t = \Delta s = 0.01$ the moving crack Γ_t^h obtained by Algorithm CT after 90 time-steps is depicted in Fig. 11a. The shadow $\Gamma_{t_k}^h(\varepsilon)$ for $\varepsilon = \sqrt{2}h$ calculated by Algorithm IS (without resharpening) with $h = 0.02$, $\Delta t = 0.002$, and $\Delta s = 0.01$ after 450 time-steps is depicted by points in Fig. 11b. For this 3D-example both algorithms perform successfully.

Acknowledgments The research results were obtained with the support of the Austrian Science Fund (FWF) in the framework of the SFB F32 "Mathematical Optimization and Applications in Biomedical Sciences" and the research project P18267-N12, and the Russian Foundation for Basic Research (project 06-01-00209).

References

1. Adalsteinsson, D., Sethian, J.A.: The fast construction of extension velocities in level set methods. J. Comput. Phys. **148**, 2–22 (1999)
2. Ambrosio, L., Soner, H.M.: Level set approach to mean curvature flow in arbitrary codimension. J. Differ. Geom. **43**, 693–737 (1996)
3. Ambrosio, L., Soner, H.M.: Flow by mean curvature of surfaces of any codimension. In: Variational Methods for Discontinuous Structures, Progr. Nonlinear Differential Equations Appl., vol. 25, pp. 123–134. Birkhäuser, Basel (1996)
4. Burchard, P., Cheng, L.-T., Merriman, B., Osher, S.: Motion of curves in three spatial dimensions using a level set approach. J. Comput. Phys. **170**, 720–741 (2001)
5. Burger, M.: A level set method for inverse problems. Inverse Probl. **47**(5), 1327–1355 (2001)
6. Burger, M., Ring, W.: Foundation of a level-set based shape sensitivity analysis (in preparation)
7. Conway, E.D.: Generalized solutions of linear differential equations with discontinuous coefficients and the uniqueness question for multidimensional quasilinear conservation laws. J. Math. Anal. Appl. **18**, 238–251 (1967)
8. Crandall, M.G., Lions, P.L.: On existence and uniqueness of solutions of Hamilton–Jacobi equations. Nonlinear Anal. T M A **10**, 353–370 (1986)
9. Delfour, M.C., Zolesio, J.-P.: Shapes and Geometries. SIAM, Philadelphia (2001)
10. DiPerna, P.J., Lions, P.L.: Ordinary differential equations, transport theory and Sobolev spaces. Invent. Math. **98**, 511–547 (1989)
11. Filippov, A.F.: Differential equations with discontinuous right-hand side. In: Amer. Math. Soc. Transl. Ser. 2, vol. 42, pp. 199–231. AMS, Providence (1964)
12. Friedman, A., Liu, Y.: Propagation of cracks in elastic media. Arch. Rat. Mech. Anal. **136**(3), 235–290 (1996)
13. Hintermüller, M., Ring, W.: A second order shape optimization approach for image segmentation. SIAM J. Appl. Math. **64**(2), 442–467 (2003)
14. Ito, K., Kunisch, K., Li, Z.: Level-set function approach to an inverse interface problem. Inverse Probl. **17**(5), 1225–1242 (2001)
15. Jiang, G.-S., Peng, D.: Weighted ENO schemes for Hamilton–Jacobi equations. SIAM J. Sci. Comput. **21**(6), 2126–2143 (2000)
16. Khludnev, A.M., Kovtunenko, V.A.: Analysis of Cracks in Solids. WIT-Press, Southampton (2000)
17. Khludnev, A.M., Ohtsuka, K., Sokolowski, J.: On derivative of energy functional for elastic bodies with cracks and unilateral conditions. Quart. Appl. Math. **60**(1), 99–109 (2002)
18. Khludnev, A.M., Sokolowski, J.: Modelling and Control in Solid Mechanics. Birkhäuser, Basel, Boston (1997)
19. Kovtunenko, V.A.: Sensitivity of interfacial cracks to non-linear crack front perturbations. J. Appl. Math. Mech. (ZAMM) **82**(6), 387–398 (2002)
20. Lions, P.L.: Generalized Solutions of Hamilton–Jacobi Equations. Research Notes Math, vol. 69. Pitman, Boston (1982)
21. Litman, A., Lesselier, D., Santosa, F.: Reconstruction of a two-dimensional binary obstacle by controlled evolution of a level-set. Inverse Probl. **14**, 685–706 (1998)
22. Osher, S., Fedkiw R.: Level Set Methods and Dynamic Implicit Surfaces. Applied Mathematical Sciences, vol. 153. Springer, New York (2003)
23. Osher, S., Sethian, J.: Fronts propagating with curvature dependent speed: Algorithms based on Hamilton–Jacobi formulations. J. Comput. Phys. **79**, 12–49 (1988)
24. Osher, S., Shu, C.-W.: High-order essentially nonoscillatory schemes for Hamilton–Jacobi equations. SIAM J. Numer. Anal. **28**(4), 907–922 (1991)
25. Petrova, G., Popov, B.: Linear transport equations with μ-monotone coefficients. J. Math. Anal. Appl. **260**, 307–324 (2001)
26. Poupaud, F., Rascle, M.: Measure solutions to the linear multi-dimensional transport equation with non-smooth coefficients. Commun. P.D.Es **22**, 337–358 (1997)
27. Rice, J.R.: First-order variation in elastic fields due to variation in location of a planar crack front. J. Appl. Mech. **52**, 571–579 (1985)
28. Sethian, J.A.: Level Set Methods: Evolving Interfaces in Geometry, Fluid Mechanics, Computer Vision, and Material Science. Cambridge University Press, Cambridge (1996)
29. Sethian, J.A.: A fast marching method for monotonically advancing fronts. Proc. Nat. Acad. Sci. **93**, 1591–1595 (1996)
30. Sokolowski, J., Zolesio, J.-P.: Introduction to Shape Optimization. Shape Sensitivity Analysis. Springer, Berlin (1992)
31. Stolarska, M., Chopp, D.L.: Modelling thermal fatigue cracking in integrated circuits by level sets and the extended finite element method. Int. J. Eng. Sci. **41**, 2381–2410 (2003)
32. Sukumar, N., Moës, N., Moran, B., Belytschko, T.: Extended finite element method for three-dimensional crack modelling. Int. J. Numer. Meth. Eng. **48**, 1549–1570 (2000)
33. Tsitsiklis, J.N.: Efficient algorithms for globally optimal trajectories. IEEE Trans. Automat. Control **40**, 1528–1538 (1995)
34. Ventura, G., Xu, J.X., Belytschko, T.: A vector level set method and new discontinuity approximations for crack growth by EFG. Int. J. Numer. Meth. Eng. **54**, 923–944 (2002)